22

FE Analysis of Evolution of Defects during Rolling

Dr. YU Hai-liang[1,2]
[1]*Key Laboratory for Advanced Materials Processing Technology of Ministry of Education, Department of Mechanical Engineering, Tsinghua University, Beijing 100084 China*
[2] *State Key Laboratory of Rolling and Automation, Northeastern University, Shenyang 110004 China*

Finite element method (FEM) has been widely employed for simulation of rolling problems, such as thermal field **[1,2]**, stress-strain field **[3]**, microstructure distribution **[4]**, rolling force **[5]**, rolling pressure distribution**[6]**, plate view shape **[7,8]**, roll deflection **[9,10]**, tracing the evolution of macrosegregation **[11]**. As the development of FEM, there are three important ways for the application of FEM in analysis of rolling problems recently. Firstly, rapid FEM, and its on-line application **[12-14]**; secondly, coupled multi-scale FEM, macro - FEM & micro - FEM & crystal - FEM, coupled the macro-deformation and microstructure evolution and texture distribution **[15-16]**; third, tracing the defects in whole rolling processes **[11, 18-21]**.
Defects might appear in materials, such as cracks, inclusions. The evolution behavior of defects in steels during rolling severely affects the rolled products quality. In this chapter, the author summed up the previous researches on the evolution of cracks and inclusions during rolling, mainly contains the researches on the evolution of surface cracks by 2D thermo-mechanical FEM, the evolution of surface cracks during vertical-horizontal (V-H) rolling by 3D FEM, the evolution of internal cracks during V-H rolling, the evolution of inclusions during flat rolling.

1. Evolution of surface cracks by 2D thermo-mechanical FEM

Since the brittle fracture model proposed by Griffith last century, a large number of researchers and engineers have carried out a lot of work that focuses on the behavior of cracks. The research reports on the appearance and the propagation of cracks in rolled steels during rolling were investigated **[22~25]**.
Considerable investigations have been carried out on applying FEM for simulation of the propagation and closure of cracks in materials during rolling. A self-healing shape memory alloy (SMA) composite was simulated via a finite element approach that allows crack to propagate in a brittle matrix material by Burton, et al **[26]**. The SMA wires were carefully

modeled using a one-dimensional SMA constitutive model and implemented into user-defined truss elements. Loading of the composite allowed a crack to propagate from an initiation site and the wires bridge the crack as detwinned martensite forms with the applied loading. Awais **[27]** and Son et al **[28]** employed the two-dimension FEM and Processing Map to analyze the closure and growth of surface crack in bars in the rolling process. Ervasti, et al **[29, 30]** simulated the closure and growth of longitudinal and transversal cracks in flat rolling process, and analyzed the closure and growth of cracks under a variety of the crack sizes, roll radii, friction coefficients, etc. Yukawa, et al **[31, 32]** analyzed the deformation of the micro-cracks, the foreign bodies pressing and so on in rolling process by a two-dimensional (2D) rigid-plastic FE code developed by them. In this part, the researches on the evolution of surface cracks by 2D thermo-mechanical FEM are carried out.

1.1 Finite element method

1.1.1 Basic theory

Eq. (1) **[33]** shows the calculation equation of thermal distribution in an isotropic element with an internal heat source.

$$\frac{\partial^2 T}{\partial x^2}+\frac{\partial^2 T}{\partial y^2}+\frac{\partial^2 T}{\partial z^2}+\frac{\dot{q}}{k}=\frac{\rho c}{k}\frac{\partial T}{\partial t} \tag{1}$$

where ρ is density; c is specific heat; k is coefficient of heat conductivity; $\dot{q}$ is internal heat source strength, which is the plastic work done of slab deformation during rolling.

$$\dot{q}=m\int_0^{\dot{\varepsilon}}\bar{\sigma}d\dot{\varepsilon} \tag{2}$$

where m is coefficient of heat transform by plastic work done, $m=0.7\sim 0.95$ **[34]**.

During hot rolling, the thermal transfers between the slab surface and the external environment contain two ways: heat emission and convection current. When the slab is not in the deformation zone, the heat radiation is much larger than the heat convection which could be neglected. According to the Stefan-Boltzman equation,

$$Q=H_r A(T-T_\infty) \tag{3}$$

where $H_r=S_B B_S(T^2+T_\infty^2)(T+T_\infty)$, S_B is the coefficient of Stefan-Boltzman; B_S is the blackness on slab surface, T is the slab surface temperature; T_∞ is the temperature of environment.

The heat transfers between the slab surface and the work roll is calculated by the Eq. (4).

$$Q=h_i A(T-T_R) \tag{4}$$

where h_i is the coefficient of convective heat transfer between the slab and the roll; T_R is the temperature of roll.

The coupled thermal-mechanical method is solved by dynamic explicit approach **[35]**.

The heat transfer equations are integrated using the explicit forward-difference time integration rule:

$$\theta_{i+1}^N=\theta_i^N+\Delta t_{i+1}\dot{\theta}_i^N \tag{5}$$

where θ^N is the temperature at node N and the subscript i refers to the increment number in an explicit dynamic step. The values of $\dot{\theta}_i^N$ are computed at the beginning of the increment by

$$\dot{\theta}_i^N=(C^{NJ})^{-1}(P_i^J-F_i^J) \tag{6}$$

where C^{NJ} is the lumped capacitance matrix, P^J is the applied nodal source vector, and F^J is the internal flux vector.
The equations of motion for the body are integrated using the explicit central-difference integration rule

$$\dot{u}^N_{i+\frac{1}{2}} = \dot{u}^N_{i-\frac{1}{2}} + \frac{\Delta t_{i+1} + \Delta t}{2} \ddot{u}^N_i \tag{7}$$

$$u^N_{i+1} = u^N_i + \Delta t_{i+1} \dot{u}^N_{i+\frac{1}{2}} \tag{8}$$

where u^N is a degree of freedom (a displacement or rotation component) at node N. The accelerations at the beginning of the increment are computed by

$$\ddot{u}^N_i = (M^{NJ})^{-1}(P^J_i - I^J_i) \tag{9}$$

where M^{NJ} is the mass matrix, P^J is the applied load vector, and I^J is the internal force vector.

1.1.2 Parameters and FE model

Fig.1 shows the schematic drawing of slab rolling with a surface crack. In the models, the work roll diameter (D_W) is 1 150 mm, the slab thickness before rolling (H_0) is 250 mm, and the slab thickness after rolling (H_1) is 230 mm. The cracks are assumed to be V-shaped. There are two important parameters for definition of the crack: crack height (H_C), and crack open-angle (θ), whose effects on the behavior of cracks during rolling are analyzed. The values of H_C are assumed to be 2 mm, 4 mm, 6 mm, 8 mm, and 10 mm respectively. The values of θ are assumed to be 5 °, 10 °, 20 °, 30 °, 40 ° separately.

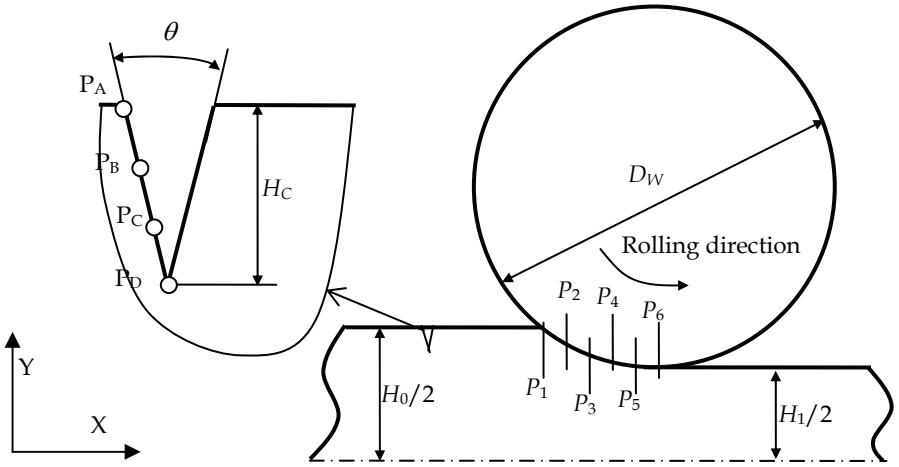

Fig. 1. Schematic drawing of slab rolling with a surface crack

The Coulomb friction model is used for solving the pressure between the crack surfaces and that between the slab and the roll. The influence of friction factor between the slab and the roll on the behavior of cracks during rolling are analyzed. The friction coefficients are assumed to be 0.2, 0.25, 0.35, 0.45, and 0.55.

The heat transfer between the slab and the roll, and between the crack surfaces are appeared, where the heat conductivity is assumed to be constant 46 W/m·K. During rolling, the deformation resistance of slab is related with the strain, strain rate, and temperature. The roll is assumed to be rigid, and the slab is isotropic bilinear model. The main material parameters are shown in **Table 1**.

Parameters	Roll	Slab
Density, kg/m^3	7830	7830
Young's modulus, GPa	210	117
Poisson's ratio	0.3	0.36
Deformation resistance, MPa	-	$\sigma = A\varepsilon^{B}\dot{\varepsilon}^{CT+D}e^{FT}$
Heat capacity, J/(kg·K)	460	460

Table 1. Material parameters (σ is stress; ε is true strain; $\dot{\varepsilon}$ strain rate; A, B, C, D, and F are constants)

Owing to the symmetry of the rolls and the slab, a half of rolling geometrical model is employed. During rolling, the width spread of slab in a local zone is small, where the behavior of cracks could be approximate as the 2D deformation, so a 2D geometrical model is used. With the parameters above, the models of slab rolling with a surface crack are established, which are meshed by the quadrilateral elements. The FE meshing of slab with a surface crack during rolling is shown in **Fig.2**. The nodes on the bottom of slab are constrained for displacement along slab thickness direction, $U_Y = 0$. During rolling, the slab enters the roll with an initial velocity, and exits under the action of friction force between the roll and the slab.

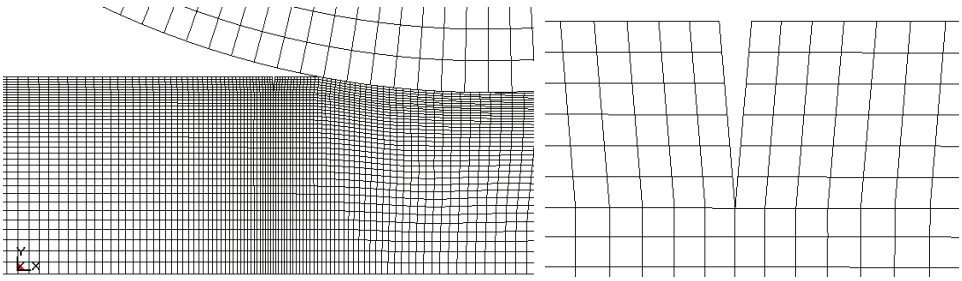

Fig. 2. Meshing of slab with a surface crack during rolling

1.2. Results and discussion [36]

1.2.1 Stress around crack tip during rolling

Fig. 3 shows the stress (σ_x) distribution around the crack at different positions in the deformation zone during rolling when the initial crack height is 10 mm, the initial crack open-angle is 10 ° and the friction coefficient is 0.35. In the bite zone, the compressive stress appears around the crack, and the crack gradually close, as shown in Fig.3 (a) ~ (c). In Fig.3 (d), the stress around crack is small, and the crack keeps its shape. When the crack is in the

forward zone, the tensile stress appears around cracks, and when the crack is at P_6, the maximum tensile stress around crack tip attaches to 900 MPa, as shown in Fig.3 (e) and (f). It is obvious that the larger the compressive stress is, the more easily the cracks close, and the larger the tensile stress is, the more easily the cracks propagate. The maximum compressive stress and the maximum tensile stress at crack tip during rolling are further analyzed as follows.

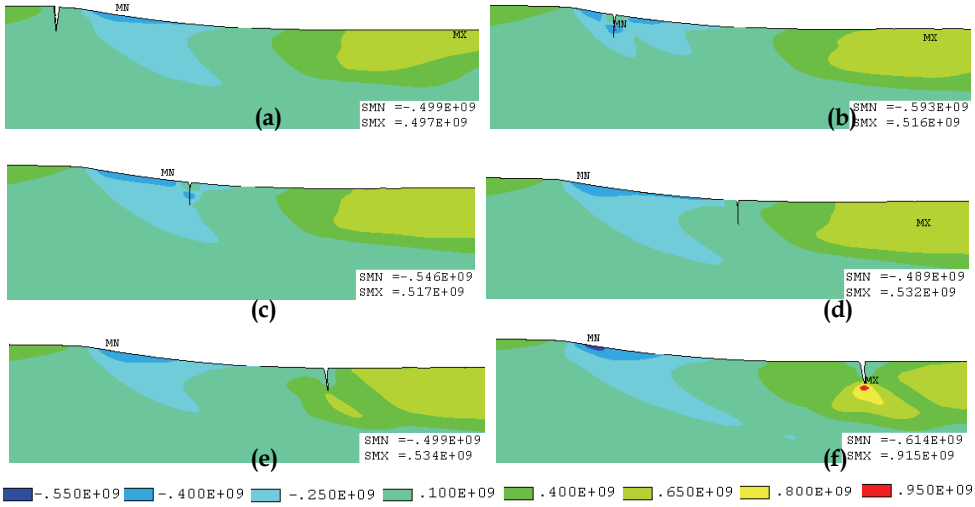

Fig. 3. Stress distribution around the crack at P_1 (a), P_2 (b), P_3 (c), P_4 (d), P_5 (e) and P_6 (f) in the deformation zone

Fig. 4 shows the maximum compressive and tensile stress at crack tip during rolling under various initial crack heights when the friction coefficient is 0.35 and the initial crack open-angle is 10 °. As the initial crack height decreases, the maximum compressive stress increases. By contraries, the maximum tensile stress increases as the initial crack height increases.

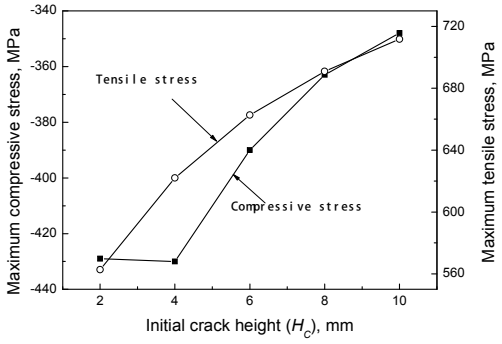

Fig. 4. Maximum compressive and tensile stress at crack tip during rolling for various H_C

Fig. 5 shows the maximum compressive and tensile stress at crack tip for a variety of initial crack open-angles when the friction coefficient is 0.35 and the initial crack height is 10 mm. With increasing the initial crack open-angle, the compressive stress increases. Under the rolling conditions, the maximum tensile stress decreases as the initial crack open-angle increases when the crack open-angle is 5~20°, which increases when the crack open-angle is between 20~40°.
Fig. 6 shows the maximum compressive and tensile stress at crack tip under different friction coefficients when the initial crack height is 10 mm and the initial crack open-angle is 10 °. The maximum compressive stress increases with decreasing the friction coefficients. The maximum tensile stress increases with increasing the friction coefficients when the friction coefficient is from 0.2 to 0.45.

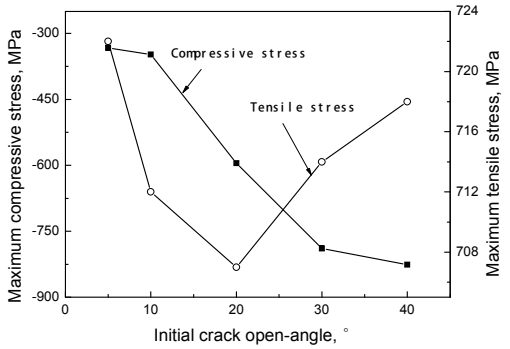

Fig. 5. Maximum compressive and tensile stress at crack tip during rolling for various θ

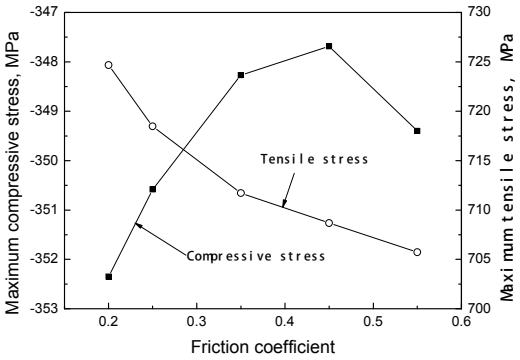

Fig. 6. Maximum compressive and tensile stress at crack tip during rolling for various friction coefficients

Compared the stress value in Figs.4, 5 and 6, the influence of the initial crack open-angle on the maximum compressive stress is the most obvious, whose difference is up to 450 MPa, and the influence of the initial crack height on the maximum tensile stress is the most obvious; the influence of the friction coefficient on the compressive stress is the slightest, and the influence of the initial crack open-angle on the maximum tensile stress is the slightest.

1.2.2 Crack open-angle and height after rolling

Fig. 7 shows the crack open-angle and the crack height after rolling under various the initial crack heights when the initial crack open-angle is 10° and the friction coefficient is 0.35. After rolling, the crack open-angle increases with reducing the initial crack height, and the crack height after rolling is direct ratio to the initial crack height.

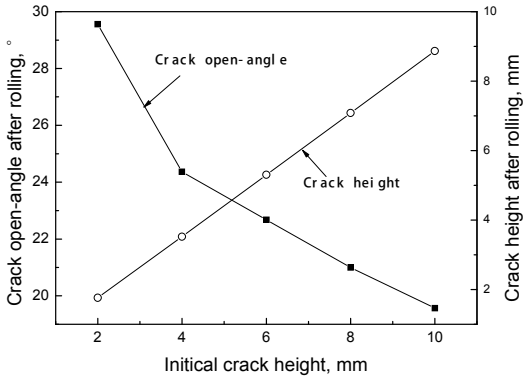

Fig. 7. Crack open-angle and height after rolling for various H_C

Fig. 8 shows the crack open-angle and height after rolling under a variety of initial crack open-angle when the initial crack height is 10 mm and the friction coefficient is 0.35. As the initial crack open-angle increases, the crack height after rolling decreases and the crack open-angle after rolling increases.

Fig. 9 shows the crack open-angle and height after rolling under various friction coefficients when the initial crack open-angle is 10° and the initial crack height is 10 mm. With increasing the friction coefficient, the crack open-angle after rolling increases and the crack height decreases.

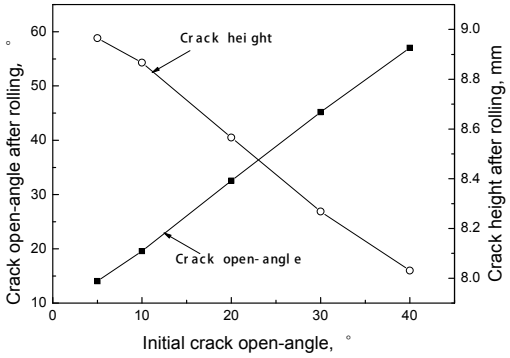

Fig. 8. Crack open-angle and height after rolling for various θ

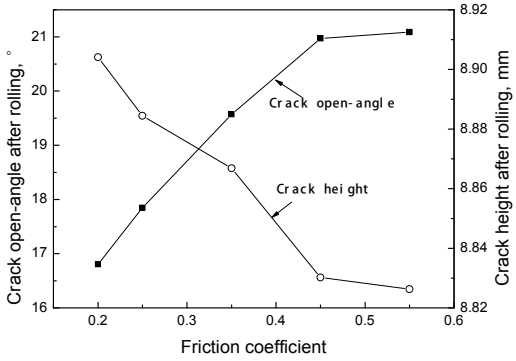

Fig. 9. Crack open-angle and height after rolling for various friction coefficients

1.2.3 Thermal distribution around crack surfaces during rolling

Fig. 10 shows the thermal distribution around the crack when the initial crack height is 10 mm, the initial crack open-angle is 10 ° and the friction coefficient is 0.35. After rolling, the temperature on crack surface is much less than that in slab matrix. It is obvious that the higher the temperature on crack surface, the more easily the behavior of crack metallurgical healing occurs under the compressive stress. So the thermal distribution around the crack will severely affect the behavior of cracks during rolling.

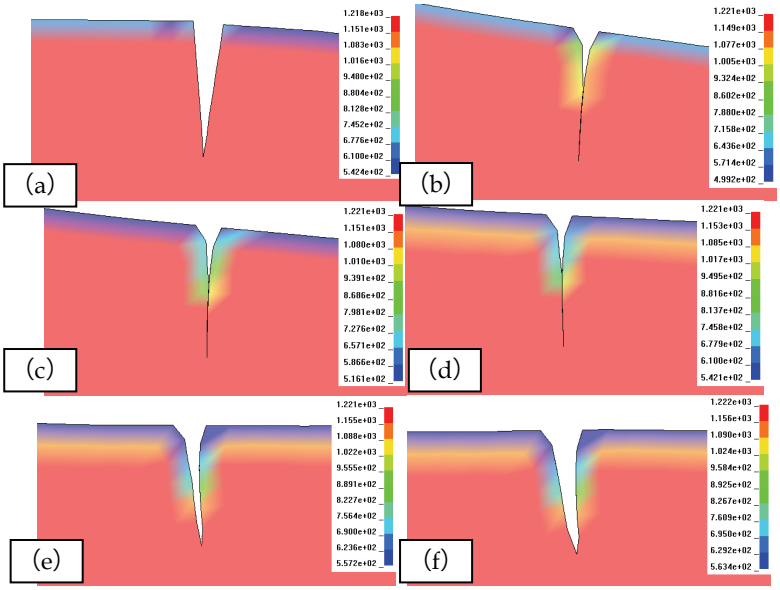

Fig. 10. Thermal distribution around crack at P_1 (a), P_2(b), P_3 (c), P_4 (d), P_5 (e) and P_6 (f) during rolling (°C)

Fig. 11 shows the temperature variation curve on crack surfaces during rolling under various initial crack heights when the initial crack open-angle is 10° and the friction coefficient is 0.35. In Fig.11 (a), the temperature in P_A changes slightly under various the crack height. As the position approaches to the crack tip, the difference between the temperatures increases. In Fig.11 (b), the temperature in P_B, when the crack height is larger than 8 mm, the temperature changes slightly, and when the crack height is less than 4 mm, the minimum temperature changes slightly and the difference increases as the rolling time increases.

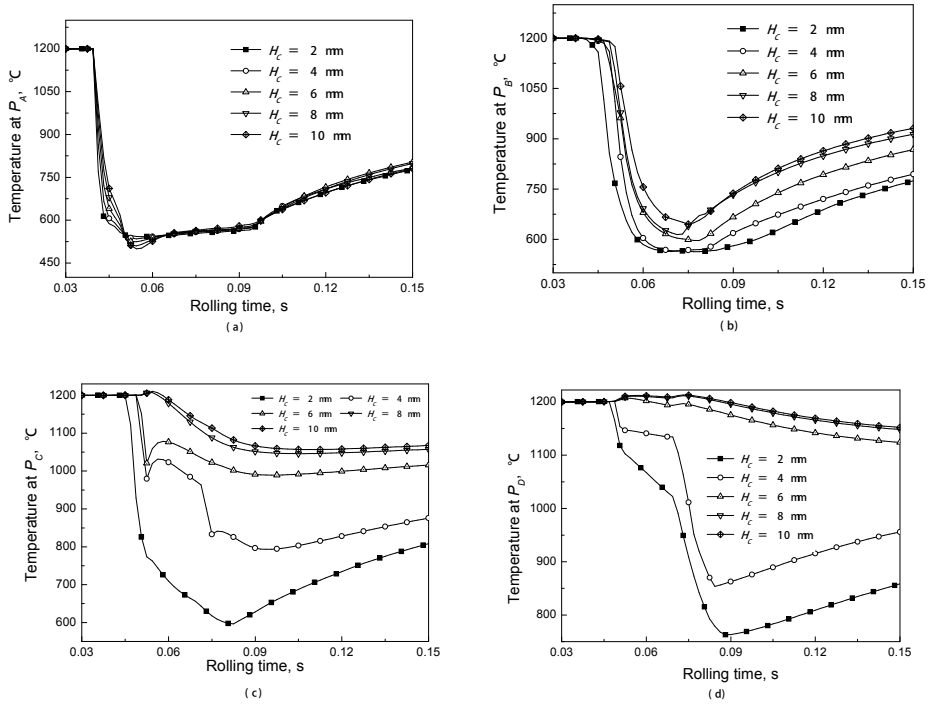

Fig. 11. Temperature at P_A (a), P_B (b), P_C (c) and P_D (d) during rolling for various H_C

In Fig.11(c), when the initial crack height is larger than 4 mm, the temperature increases in the deformation zone, and the temperature directly decreases to minimum temperature in the deformation zone when the initial crack height is 2 mm. In Fig.11 (d), there are two peaks of temperature in the deformation zone when the initial crack height is larger than 6 mm, and the temperature variation is less than 100 ℃. When the initial crack height equals to 2 mm, the temperature variation approaches 450 ℃.

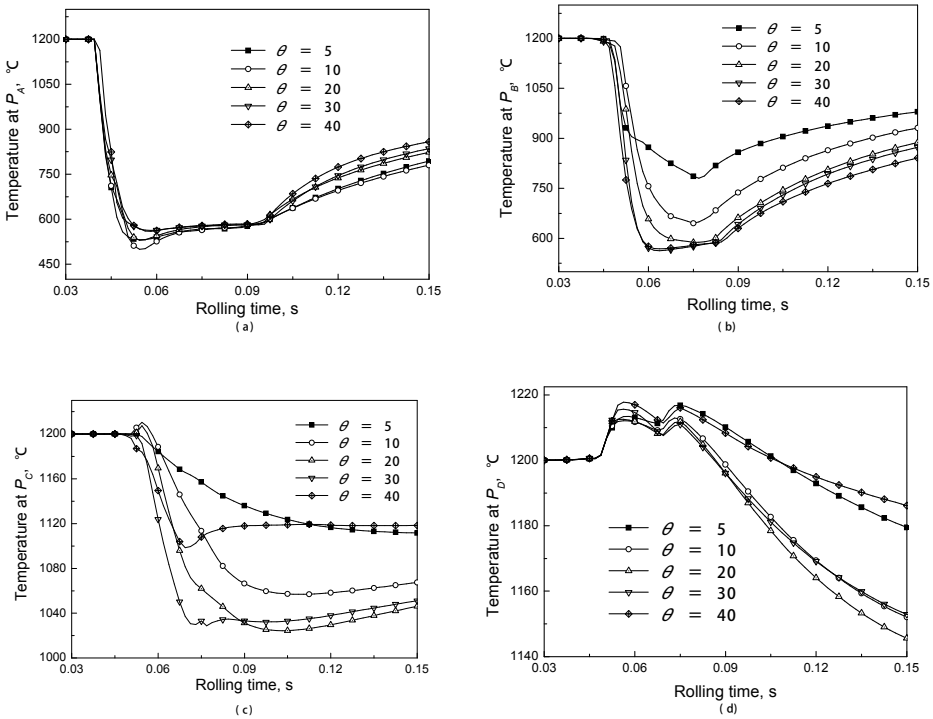

Fig. 12. Temperature at P_A (a), P_B (b), P_C (c) and P_D (d) during rolling for various θ

Fig. 12 shows the temperature variation curve on crack surface under a variety of initial crack open-angles when the initial crack height is 10 mm and the friction coefficient is 0.35. In Fig.12 (a), the temperature varies slightly in the deformation zone, and after rolling, the heating-up speed increases as the crack open-angle increases when it is greater than 10°. In Fig.12 (b), the temperature drop decreases with decreasing the initial crack open-angle. The minimum temperature is about 800℃ when the initial crack open-angle is 5°, and the minimum temperature is about 550 ℃ when the initial crack open-angle is 40°, the difference attaches to 250℃. In Fig.12(c), the temperature drop increases with increasing the initial crack open-angle when they are less than 20 °, which decreases when they are larger than 20 °, that is caused by the plastic work done. In Fig.12 (d), the temperature variation among them is less than 100℃, and they have the same regularity as that in Fig.12(c).

Fig. 13 shows the temperature variation curve on crack surfaces during rolling under various friction coefficients when the initial crack height is 10 mm and the initial crack open-angle is 10°. The temperature on crack surface varies slight during rolling except that the friction coefficient is 0.2. And the temperature rises with increasing the friction coefficient.

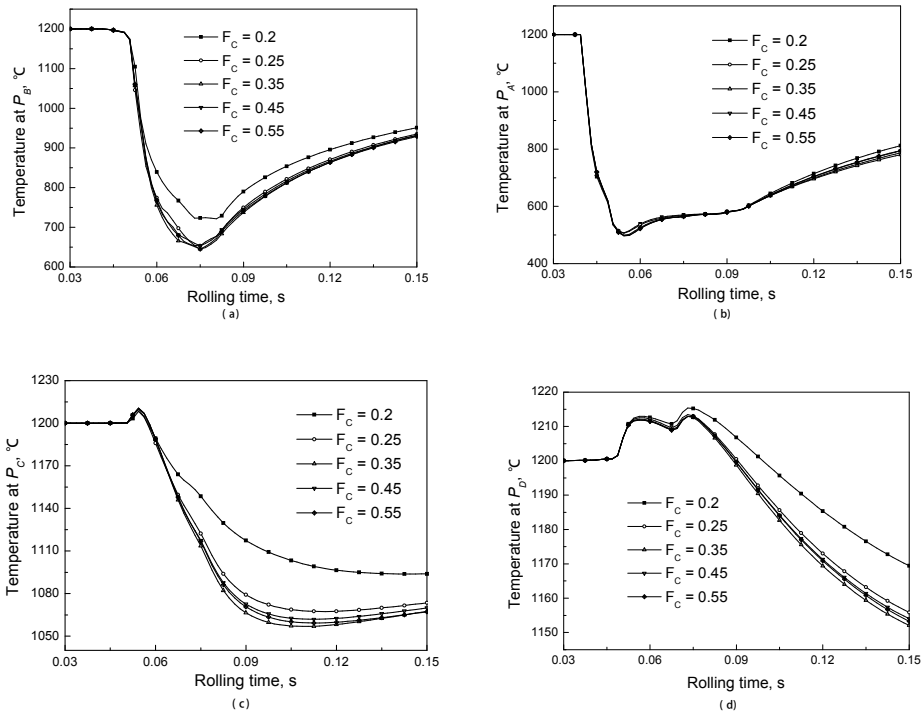

Fig. 13. Temperature at P_A (a), P_B (b), P_C (c) and P_D (d) during rolling for various friction coefficients

From the results above, the cracks close in the bite zone of deformation zone during rolling. The compressive stress appears on the crack surfaces. Then the crack might be healing under the conditions. In the forward slipping zone of deformation zone during rolling, the tensile stress appears around the cracks. When the tensile stress is less than the metallurgical bonding strength, the cracks will not open again, so after a pass, part of cracks heals, then as the rolling passes increase, the cracks gradually close after rolling, as shown in **Fig.14**(a). When the tensile stress makes part of healing zone open again, the position of P_X might move to the slab surface, after lots of rolling passes, part of cracks heals, and part of cracks becomes the slab surfaces, as shown in **Fig.14** (b). When the tensile stress makes the healing part open again, and the crack open-angle is larger than the crack open-angle before rolling, and the crack height decreases after rolling. As the rolling pass increases, the crack surfaces become the slab surface wholly, as shown in **Fig.14**(c).

The cracks might heal when the temperature is enough high **[37, 38]**, and the influence of thermal and stress distribution around cracks is very important. When the temperature of crack surface is quite low, the metallurgical bonding strength on crack surfaces will decrease severely. As shown in Fig. 11, the temperature distribution on the whole crack surface during rolling is lower than 800 ℃ when the initial crack height is 2 mm, so the cracks can not heal during rolling. Meanwhile, the crack open-angle after rolling is 29.5° whose initial

crack open-angle is 10°. As the rolling passes increase, the cracks open whole and become part of slab surfaces, as shown in Fig.14 (c). As shown in Fig. 12, the temperature of in P_C and P_D are larger than 1000℃, and the cracks might repair themselves under compressive stress, as shown in Fig.14 (b), even the whole cracks close as shown in Fig.14 (a).

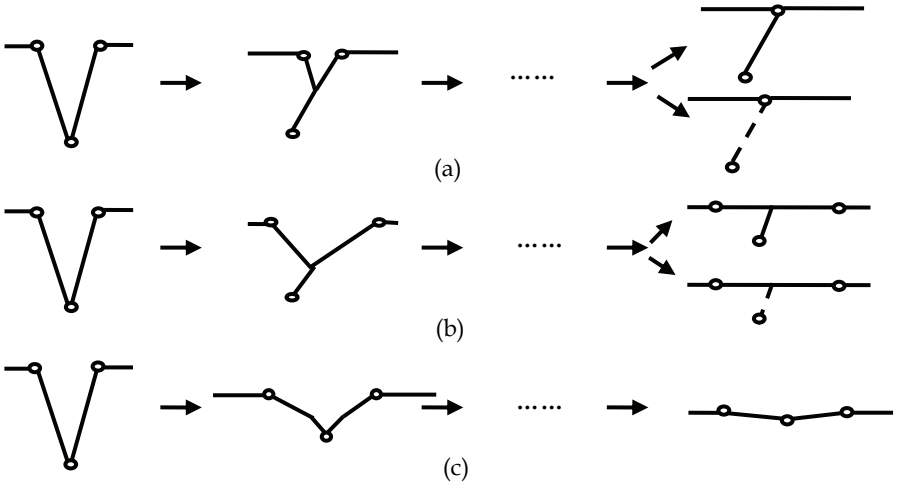

Fig. 14. Schematic of behavior of cracks on slab surface during rolling

2. Evolution of surface cracks on slab corner and edge by 3D FEM

The vertical-horizontal (V-H) rolling has been widely used for adjustment of the slab width for connection between the continuous casting and the finish rolling process. The deformation behavior of slab during rolling affects the quality of rolled steel. The FEM has been widely used for simulation of the behavior of slab during V-H rolling. The behavior of slab during V-H rolling was simulated by Xiong et al with the thermal-mechanical coupled rigid-plastic FEM **[39]**, the thermal distribution and the strain distribution of slab during rolling were obtained, and the unsteady head and tail of slab were analyzed which were in good agreement with those of experimental ones. The three-dimensional rigid plastic/visco-plastic FEM was employed to simulate the behavior of slab during vertical rolling, the slab shape and the rolling force during rolling were obtained that were in good agreement with the experimental ones **[40]**. The behavior of slab during multi-pass V-H rolling was simulated by the author, and the shape of head and tail of slab during horizontal rolling with different dog-bone shape was also analyzed **[41]**. In this part, the researches on the evolution of surface cracks on slab corner and edge by 3D FEM were carried out.

2.1 Basic methods of analysis and assumptions

2.1.1 Explicit dynamic FEM

The fundamental equation of explicit dynamic element method **[42]** is

$$M\ddot{u} + C\dot{u} + F = R \tag{10}$$

Compared with static analysis, the mass matrix and damping matrix are introduced into equilibrium equation of dynamic analysis because of the existence of inertia force and damping force. The final solution equations are ordinary differential equation groups instead of algebraic ones. Generally, the Eq. (10) can be obtained by integrating central difference interpolation, which belongs to immediate integration method. In this method, the discrete velocity and acceleration at t_n can be expressed as:

$$\dot{u}_n = \frac{1}{2\Delta t}(u_{n+1} - u_{n-1}) \tag{11}$$

$$\ddot{u}_n = \frac{1}{\Delta t^2}(u_{n+1} - 2u_n + u_{n-1}) \tag{12}$$

Substituting the Eq.(11) and Eq.(12) into Eq.(10), the discrete-time recurrence equation is obtained as following:

$$u_{n+1} = [M + \frac{\Delta t}{2}C]^{-1}[\Delta t^2(R_n - F_n) + 2Mu_n - (M - \frac{\Delta t}{2}C)u_{n-1}] \tag{13}$$

The central difference method is stable under certain condition that the time step Δt must be lower than $\Delta t_{\min}$. Otherwise, the algorithm will be unstable. Generally, according to the Courant-Friedrichs-Levy stability criterion, the critical time step value is:

$$\Delta t_{\min} = \frac{2}{w_{\max}} = \frac{l}{c} \tag{14}$$

For 3D element, the sound velocity in the material is:

$$c = \sqrt{\frac{(1-\nu)E}{(1+\nu)(1-2\nu)\rho}}. \tag{15}$$

2.1.2 Contact problem of crack surfaces

In rolling process, the contact problems between the slab and the rolls, between the crack surfaces are the surface to surface problems, which are solved with the penalty function algorithms. The contact stiffness (k) is determined by the Eq. (16)**[43]**.

$$k = \frac{f_s \times A_E^{\,2} \times K}{V_E} \tag{16}$$

Where, f_s is the penalty factor, which equals 0.1 here;

A_E is the area of contact segment;

V_E is the element volumes;

K is the bulk modulus of contacted element. Where $K = \frac{E}{3(1-2\sigma)}$, E is Young's modulus, and σ is the Poisson's ratio.

2.1.3 Multi-pass rolling process simulation

The updating geometrical method**[44]** is employed to simulate the multi-pass rolling processes with a single pass rolling process FE model, which is that adding displacements from the previous analysis results and updating the geometry of the finite element model to

the deformed configuration. The updating geometrical process of rolling processes is shown in **Fig. 15**.

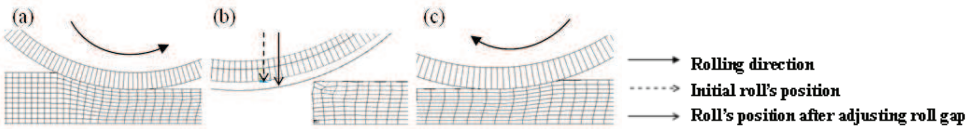

Fig. 15. Updating geometrical process of rolling process

2.1.4 Assumptions

In the research of the closure and growth of crack, there are two assumptions:
(1) The crack is made up of two surfaces;
(2) The crack is "V"-shape **[29, 30]** which exists on slab corner;
(3) The height of the crack on top surface equals to that on side surface of slab.

2.2 Evolution of corner cracks during rolling

2.2.1 Basic parameters and rolling conditions

The closure and growth of crack during multi-pass V-H rolling process (V_1-H_1-V_2-H_2-V_3-H_3)**[44]** has been simulated. In the simulation, the diameter of horizontal roll is 1 150mm. The edger roll of 980mm in diameter separately employs the flat edger roll and the grooved edger roll whose dimensions are shown in **Fig.16**, where the groove fillet radius R equals to 30, 50, 80 and 110mm. The initial dimension of slab profile is 1 200×250mm.The "V"-shape cracks on slab corner are regarded as two surfaces. The crack size (crack height on slab top surface-crack height on slab side surface-crack width) employs 20-20-2（**Fig.17**）, 15-15-1.5, 10-10-1, 5-5-0.5mm respectively.

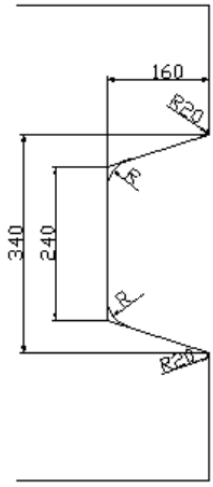

Fig. 16. Dimensions of grooved edger roll

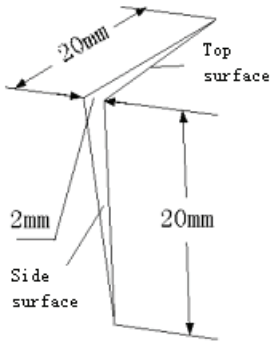

Fig. 17. Dimensions of one kinds of crack with "V"-shape

In this simulation, the rolls are assumed to be rigid and the slab is modeled as bilinear isotropic. The bilinear isotropic model is shown in Eq. (18).

$$\sigma_Y = \sigma_0 + E_P \varepsilon_P^{eff} \tag{18}$$

Where, σ_0 is the initial yield resistance;

ε_P^{eff} is the effective plastic strain;

E_P is the plastic hardening modulus.

The main chemical compositions of slab are (mass %): C 0.18, Si 0.32, Mn 0.82. The yield stress at the high temperature related to the true strain ε, the true strain velocity $\dot{\varepsilon}$, and the deformation temperature T. During this simulation, the initial yield stresses were computed by Eq. (19).

$$\sigma = \mathrm{A}\varepsilon^{\mathrm{B}}\dot{\varepsilon}^{CT+\mathrm{D}}\mathrm{e}^{FT} \tag{19}$$

where A, B, C, D, F are constants, as shown in **Table 2**.

Coefficient	A	B	C	D	F
Value	1715.706	0.17311	0.16952	0.05515	-0.267881

Table 2. Coefficients in the initial yield stress model

In the simulation, the main material parameters are shown in **Table 3**.

Parameters	Roll	Slab
Young's modulus, GPa	210	117
Poisson's ratio	0.3	0.36
Density, kg/m^3	7850	7850
Plastic hardening modulus, MPa	-	10.1
Initial yield stress, MPa	-	Eq. (19)

Table 3. Basic material parameters in rolling process

During rolling process, the draft of vertical rolling in every pass is 50mm, and the draft of horizontal rolling is 10mm. In this paper, there are 18 kinds of simulation schedules, which are shown in **Table 4**.

Schedule	E-roll shape	R/mm	Crack size /mm	*f*
1	Flat	—	20-20-2	0.25
2	Flat	—	20-20-2	0.35
3	Flat	—	20-20-2	0.45
4	Flat	—	20-20-2	0.55
5	Groove	50	20-20-2	0.25
6	Groove	50	20-20-2	0.35
7	Groove	50	20-20-2	0.40
8	Groove	50	20-20-2	0.43
9	Groove	50	20-20-2	0.45
10	Groove	50	20-20-2	0.47
11	Groove	50	20-20-2	0.50
12	Groove	50	20-20-2	0.55
13	Groove	50	15-15-1.5	0.35
14	Groove	50	10-10-1	0.35
15	Groove	50	5-5-0.5	0.35
16	Groove	30	20-20-2	0.35
17	Groove	80	20-20-2	0.35
18	Groove	110	20-20-2	0.35

Table 4. Simulation schedules and rolling conditions

2.2.2 Establishment of models

Owing to the symmetry of slab and rolls, 1/4 of slab and rolls were included in the geometric model. According to the parameters mentioned above, the rolling model of the first pass was built. The rolls were considered as rigid because their deformation could be neglected. The whole geometric model was meshed with 8 nodes and hexahedral elements. At the same time, it just refined the elements near the slab margin where the deformation assembled. The nodes on the bottom face of slab were constrained along Y direction, U_y=0; and the nodes on the center face of slab were constrained along Z direction, U_z=0. The geometrical model and meshing of slab with crack before rolling was shown in **Fig.18**. During simulation, the slab entered the rolls with an initial velocity and exited the rolls under the friction force. The rolling models of the 2nd and the 3rd passes were obtained by updating geometry, changing material attribution, boundary conditions and loads.

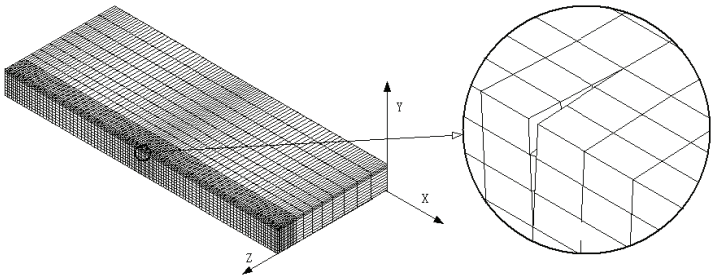

Fig. 18. Geometry and meshing of slab with crack

2.2.3 Results and analysis [45]

The deformation behavior of crack could be realized through the analysis of the change of the crack width during rolling process, which may be used to do the qualitative analysis of the closure and growth of crack. Meanwhile, when the crack closes, two surfaces of the crack will contact each other and appear contact pressure. The contact pressure between crack surfaces may be used to analyze the contact strength for crack surfaces which can be employed to analyze which method is more helpful for the crack closure. However, when the crack is growing or open, the contact pressure will become zero, then, it can't support help for researching. In this paper, the crack width and the contact pressure on crack surfaces at the exit stage of rolling are used to analyze the behavior of transversal crack on slab corner during multi-pass V-H rolling process.

(1) Influence of the friction coefficient on the crack's closure and growth

1> Flat edger roll

When the flat edger roll is used during multi-pass V-H rolling process, after horizontal rolling, the transversal crack on slab corner may close. During following it just analyzes the closure and growth of transversal crack during V_1-H_1 rolling process. And the simulation schedules 1~4 as shown in **Table 4** are adopted.

<1> Crack width

Fig.19 shows the influence of the friction coefficient on the crack width during V-H rolling process when the flat edger roll is used. In vertical rolling, the influence of friction coefficient on crack width is little, and when the friction coefficient is among 0.25~0.55, the cracks width all are less than 0.25mm. But during horizontal rolling process, the influence of the friction coefficient on crack width is very obvious. When the friction coefficient changes among 0.25~0.35, the cracks close, and when the friction coefficient changes among 0.35~0.55, the final crack width increases gradually with the increasing of the friction coefficient.

<2> Contact pressure

Fig.20 shows the influence of the friction coefficient on the contact pressure on crack surfaces on slab corner during V-H rolling process when the flat edger roll is used. It is very clear that the value of contact pressure in vertical rolling is much larger than that in horizontal rolling. During vertical rolling process, with the changing of friction coefficient, the contact pressure varies among 50~70MPa. And with the increasing of friction coefficient, the contact pressure decreases. During horizontal rolling process, with the increasing of friction coefficient, the contact pressure decreases acutely, from 45MPa to 0MPa, and the crack opens again.